Experimental Study of Slug Flow for Condensation in a Square Cross-Section Micro-Channel at Low Mass Velocities

Georges EL ACHKAR [1,*], Marc MISCEVIC [2], Pascal LAVIEILLE [2]

* Corresponding author: Tel.: +33 (0)491106890; Fax: +33 (0)491106969; Email: georges.elachkar@univ-amu.fr
[1] Aix-Marseille University – IUSTI, UMR CNRS 7343 – Marseille Cedex 13, France
[2] Paul Sabatier University – LAPLACE, UMR CNRS 5213 – Toulouse Cedex 9, France

Abstract In this paper, condensation flows in a cross-flow air-cooled micro-condenser were investigated for mass velocities (representing the mass flow rates over the micro-condenser cross-section area) lower than 12 $kg.m^{-2}.s^{-1}$, with n-pentane used as the working fluid. This micro-condenser consisted of a transparent square cross-section micro-channel placed horizontally, having inner and outer edges of 553 and 675 μm, respectively, and a real length exposed to the coolant of 196 mm. One of the specificities of the experimental bench was the choice of the air as a coolant so that the external heat transfer is limiting. Three main flow zones were identified: annular zone, intermittent (i.e. elongated bubbles or slug) zone and spherical bubbles zone. A specific experimental procedure based on bubbles tracking was developed in order to determine the hydraulic and thermal parameters in the intermittent zone. The mean displacement and condensation velocities of the elongated bubbles were determined according to their mean length for different mass velocities of the n-pentane. Besides, the mean latent heat flux density released by the condensation of the elongated bubbles was determined according to their mean surface for different mass velocities of the n-pentane, and compared to the imposed heat flux density.

Keywords: Condensation, Micro-channel, Square Cross-Section, N-Pentane, Flow Patterns, Elongated Bubbles, Heat Transfer

1. Introduction

The increase integration of the electronic systems in the satellites results obviously in an increase of the dissipated heat fluxes. The areas of the satellites radiative panels become thus insufficient, leading to a thermal control problem of the electronic systems. One solution to solve this problem is to increase the radiation temperature of the satellites panels using heat pumps.

In the off-nominal operation of these heat pumps, very low mass velocities of the working fluid may be encountered. However, most of the studies on the condensation flows available in the literature were carried out at high mass velocities of several hundreds of $kg.m^{-2}.s^{-1}$, and concerned particularly the flow regimes and the heat transfer. Studies on the condensation flows at much lower mass velocities are thus required [2-4,9,10].

The conditions under which the condensers operate affect significantly the performance and the stability of the heat pumps. The gravitational field greatly influences the distribution of the liquid and vapor phases in the condensers. In a space application context, it is important to operate under a condition of low gravity impact. A possible solution, in terrestrial environment, is to reduce the size of the channels [9].

For two-phase condensation flows inside channels, the heat transfer laws are directly related to the local distribution of the vapor and liquid phases [10]. Three main flow regimes were mainly identified in the literature for various channel diameters, shapes and refrigerants: the annular regime, the elongated bubbles (i.e. slug) regime and the spherical bubbles regime [1,5,7,8,11,12].

A previous study was conducted on the spherical bubbles regime during condensation flows inside a square cross-section micro-channel [4]. In this paper, the purpose is to investigate the elongated bubbles regime from the hydraulic and thermal points of view

during condensation flows inside the same square cross-section micro-channel.

2. Experiments

2.1. Experimental Apparatus

The test rig consists mainly of an entrance tank connected to a refrigerated bath, a temperature controlled enclosure, a micrometric valve, a test section, an exit tank, a precision balance, an air conditioning system, a high-speed camera and a data acquisition system (Fig. 1). Details of the setup are available in the reference [2].

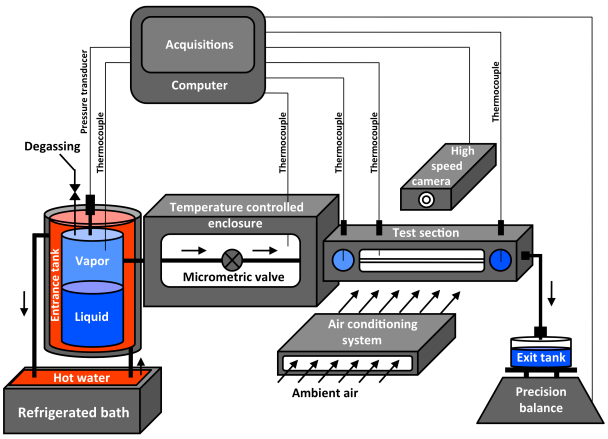

Fig. 1: Scheme of the experimental apparatus.

The role of the entrance tank is to provide saturated vapor at constant temperature and pressure. This tank contains a liquid-vapor mixture of the working fluid, which is the n-pentane having a saturation temperature of 36.06 °C at atmospheric pressure, whose temperature is controlled by a thermostated water circulation. In order to maintain a constant vapor flow rate in the test section, nozzling is provided in the micrometric valve placed in a temperature controlled enclosure maintained at 40 °C above the saturation temperature of the working fluid. Downstream of the micrometric valve, the vapor flows into the test section. This latter consists of a borosilicate horizontal square cross-section micro-channel, having inner and outer edges respectively of 553 and 675 mm, and an effective length exposed to the coolant (i.e. the air) equal to 196 mm. An air conditioning system blows the air perpendicularly to the test section with a nearly uniform velocity at the room temperature maintained constant during all the experiments. The mass flow rate of the working fluid during the experiment is measured by weighing the condensates in the exit tank, which is exposed to the ambient air (i.e. atmospheric pressure). Calibrated K-type thermocouples were implemented at several points along the working fluid circuits, in order to supervise accurately the temperature evolution of the working fluid between the entrance and the exit tanks. All the acquisitions were collected by a National Instrument data logger compact Rio. The monitoring and the control of the data were managed on Labview.

2.2 Experimental procedures

Prior to the experimental campaign, the external heat transfer coefficient between the air and the external walls of the micro-channel was determined using a specific technique based on the Laser Induced Fluorescence (LIF) and detailed in the reference [2]. A value of 294 $W.m^{-2}.K^{-1}$ was obtained with an uncertainty of ±15 %. An evaluation of the order of magnitude of the different thermal resistances between the working fluid and the air shows that the air-side heat transfer is limiting. Hence, the global heat transfer coefficient may be reasonably assumed to be equal to the external one. Afterwards, the n-pentane in the entrance tank was well degassed. A suitable mass velocity of the n-pentane was imposed in the test section by regulating the handle of the micrometric valve. The study of the different flow structures required the entire condensation process in the micro-channel to be viewed. Therefore, the experiments were limited to a maximum mass velocity of 12 $kg.m^{-2}.s^{-1}$. When the stability of the experimental conditions (e.g. mass flow rate, inlet and outlet temperatures in the test section, air temperature, etc.) was reached, a series of videos of the entire condensation zone was recorded using a high-speed camera mounted on three directions adjustable trolley. The frame rate of the camera was chosen at 2000 frames per second, in order to detect accurately the interface evolution. The

acquisition window width consisted of 1024 columns of pixels. Therefore, two different lenses were mounted on the camera according to the phenomenon that should be captured. The first one had a high magnification of 112.9 pixel.mm^{-1}, while the second one had a smaller magnification of 24.87 pixel.mm^{-1}. The uncertainty of acquisition, taking into account the space discretization by the pixels of the camera, was estimated at ±2 pixels. Finally, the recorded videos were processed using Matlab software, in order determine the phases distribution along the condensation zone inside the micro-channel.

2.3 Flow zones

The figure 2 shows an example of the different flow structures observed during a condensation flow of the n-pentane with a mass velocity of 5 kg.m^{-2}.s^{-1}. Three images corresponding to different instants were reported in this figure, highlighting the presence of three flow structures: the annular structure, the elongated bubbles (i.e. Taylor bubbles) structure and the spherical bubbles structure. These structures are qualitatively the same for all the mass velocities of the n-pentane considered in this study.

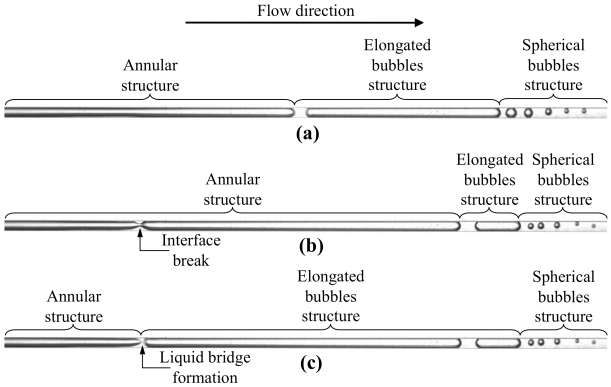

Fig. 2: Flow structures observed during a condensation flow of the n-pentane with a mass velocity of 5 kg.m^{-2}.s^{-1} at three different instants: (a) t = 0 ms, (b) t = 50 ms and (c) t = 51 ms.

For the annular structure, a thin liquid film is present along the internal circumference of the micro-channel. The vapor flows in the center and occupies almost the entire section of the micro-channel. Owing to the instabilities present in the considered type of flow, the annular structure ends with a liquid bridge formation (Fig. 2c) caused by the contact between the waves in the upper and lower parts of the micro-channel (Fig. 2b). At the instant of the interface break, an elongated bubble is released with a length (according to the micro-channel axis) of few tens of times the hydraulic diameter of the micro-channel. Referring to Garimella et al. [6], the elongated bubble has almost a square cross-section when flowing inside a square cross-section micro-channel, with an edge equal to 90 % of the micro-channel inner edge. This bubble, ending with two almost hemispherical menisci, condenses very quickly and becomes spherical when its length reaches 90 % of the micro-channel inner edge, and continues its condensation until its complete disappearance.
We define in the following the annular zone as the zone of the micro-channel where only the annular structure is present over time. This zone is almost the same as the two-phase zone situated between the micro-channel entrance and the mean position of the liquid bridges formation. Indeed, as the standard deviation of this mean position is very weak, the minimum position of the liquid bridges formation may be confused with its mean position. The same definition is considered for the spherical bubbles zone. Hence, this zone is defined by the two-phase zone situated between the axial position beyond which no presence of any elongated bubble is detected and the end of the condensation zone. Finally, the intermittent zone (i.e. elongated bubbles zone) is the remaining part of the condensation zone. Hence, the intermittent zone is the two-phase zone where all the elongated bubbles are present over time, with a possible presence at a given instant of the annular and/or the spherical bubbles structures in this zone.

2.4 Treatment procedure

In order to determine the hydraulic and thermal flow parameters in the intermittent zone, a specific experimental technique based on the Lagrangian tracking of the bubbles was developed [4]. A specific program based on Matlab was realized in order to process the

videos acquired (as sequences of images) by the high-speed camera. In order to determine the real length (according to the micro-channel axis) of each bubble, the vapor presence location along the micro-channel part observed in the acquisition window must be first identified. The developed program allowed recognizing whether a white zone detected inside the micro-channel corresponded to a liquid zone or to a vapor zone (Fig. 3a), and colored it in blue or in red, respectively (Fig. 3b). It should be noted that the white cavities that belong to the walls and outside the micro-channel were also colored in red even there was no vapor. However, these zones were not taken into account in the calculation of any flow parameter. Then, a local curve was determined for each image, indicating the presence or absence of the vapor in each position along the micro-channel part (Fig. 3c). Hence, a matrix was supplemented with 0 or 1 when the micro-channel cross-section was totally or partially filled with liquid, respectively. The row and column numbers of this matrix represented, respectively, the image number (i.e. the time) and the axial position in the micro-channel.

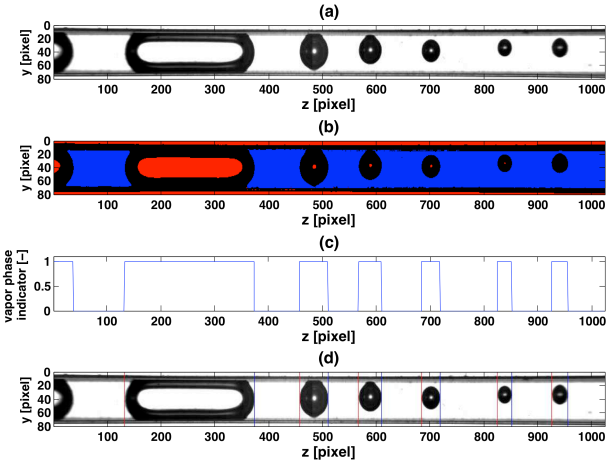

Fig. 3: Example of the detection of the vapor presence in the micro-channel; (a) original image; (b) image processing; (c) vapor phase indicator; (d) validation of the bubbles detection procedure.

The figure 4 shows the matrix of 0 and 1 in white and black colors, respectively, corresponding to a short acquired video (of 250 images) for a condensation flow of the n-pentane with a mass velocity of 5.5 $kg.m^{-2}.s^{-1}$. The black color indicates the presence of the vapor in the micro-channel part, corresponding to the presence of complete and incomplete bubbles, for all the images of the acquired video. It should be noted that in a circular cross-section channel, the glass walls curvature induces a distortion of the image, which alters the observed dimensions of the bubbles. However, in a square cross-section channel, the flatness of the glass walls preserves the dimensions of the bubbles on the resulting images.

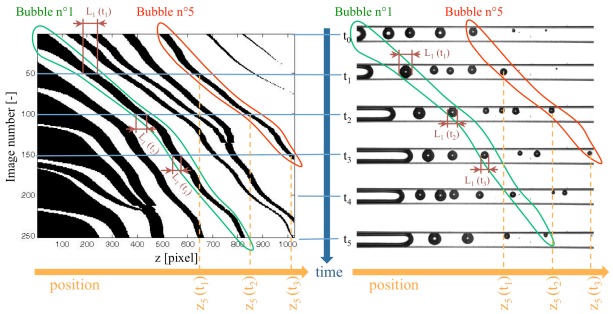

Fig. 4: On the left: example of a matrix corresponding to a short acquired video for a condensation flow of the n-pentane with a mass velocity of 5.5 $kg.m^{-2}.s^{-1}$. On the right: example of 6 images acquired at different instants and illustrating the link between the matrix and the video images.

Once the matrix was filled, the length of the micro-channel part was scanned backwards from the end to the beginning for the first row of the matrix. Hence, the bubbles lengths and centers positions were easily determined (Fig. 3d). Besides, a specific number was affected to each bubble. By iteration, the same procedure was applied to all the following rows. The bubbles positions were compared between each two successive images. If a bubble has moved below an arbitrarily chosen number of pixels, the bubble keeps the same number in both images, else, the bubble gets a new number (e.g. when a new bubble enters the micro-channel). At the end of this first step, two main matrices were created: the first matrix contained the length evolution of each bubble number (represented by a column of the matrix) as a function of the image number (represented by a row of the matrix). The

second matrix contained the evolution of the position of the bubble center (represented by a column of the matrix) as a function of the image number (represented by a row of the matrix). In a second step, these two matrices were used together in order to determine the lengths of all the bubbles passing by each cross-section of the channel. To this end, the first cross-section was chosen at the beginning of the micro-channel (i.e. at the pixel number 1), and was shifted one pixel by one pixel until the end of the micro-channel (i.e. the pixel number 1024). Considering each of these cross-sections, the total number and the lengths of the bubbles passing by this cross-section were determined.

3. Results and discussion

The mean (i.e. Eulerian) values of the void fraction and the vapor quality cannot be calculated in the major part of the intermittent zone, where the meniscus of the annular structure is present. Hence, the thermo-hydraulic study in this zone concerns exclusively the Lagrangian tracking of the elongated bubbles. In order to study the mechanisms dominating the condensation of these elongated bubbles, the temporal evolutions of their lengths and displacement velocities were determined using the experimental procedure detailed previously. The figure 5 shows the evolutions of the mean displacement velocity of the elongated bubbles as a function of their mean length for different mass velocities of the n-pentane. A very good reproducibility of the results is highlighted, regardless of the mass velocity of the n-pentane. The elongated bubbles have almost the same mean length of 30 mm at the instants of their detachments for all the mass velocities of the n-pentane. The mean displacement velocity of the elongated bubbles is maximum just after their detachments, and decreases progressively with the decrease of their mean length. It should be noted that the mean displacement velocity of the elongated bubbles is lower than the mean displacement velocity of the liquid bridges following these bubbles. This aspect can be explained by the low mean displacement velocity of the right menisci of the elongated bubbles in comparison with their left menisci mean displacement velocity (Fig. 2), resulting from the phase change occurring at these bubbles interfaces during their displacements. Hence, as the decrease of the bubble length is governed by the phase change, the evolution of the bubble displacement velocity as a function of its length can be explained as following: when the annular structure interface breaks, the overall liquid bridge and elongated bubble is pushed by the vapor situated at the hemispherical meniscus closing the annular structure. As soon as this overall moves forward in the channel, the vapor situated at this hemispherical meniscus condenses progressively, and its mass flow rate decreases. Assuming that the void ratio remains approximately constant at the end of the annular structure, the decrease of the vapor velocity at this position leads to a gradual decrease of the bubble displacement velocity.

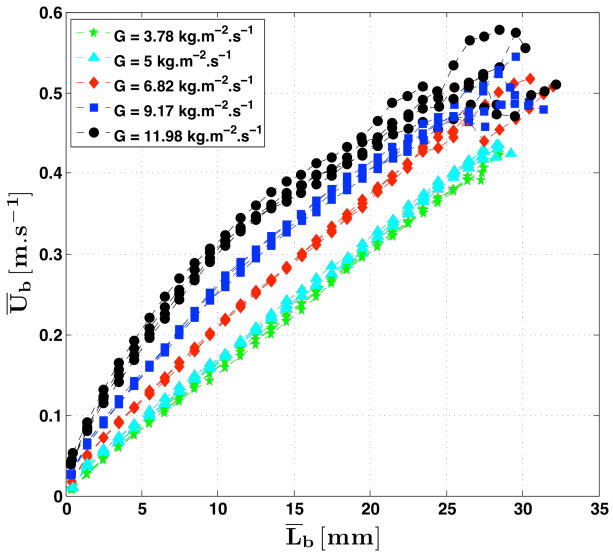

Fig. 5: Evolutions of the mean displacement velocity of the elongated bubbles as a function of their mean length for different mass velocities of the n-pentane.

The figure 6 shows the evolutions of the mean decrease (i.e. condensation) velocity of the elongated bubbles as a function of their mean length for different mass velocities of the n-pentane. The mean decrease velocity of the elongated bubbles is maximum just after their detachments, and decreases linearly with the

decrease of their mean length. Indeed, at the instant of each elongated bubble detachment, the heat exchange surface (i.e. the interface surface) between this bubble and the surrounding liquid is important, leading to a phase change rate relatively high and hence to an important bubble decrease velocity. As soon as the elongated bubble condenses, its interface area decreases, leading to a decrease of the phase change rate and hence to a reduction of the bubble decrease velocity. Besides, a slight influence of the n-pentane mass velocity on the decrease kinetics of the elongated bubbles is highlighted. Indeed, by increasing the n-pentane mass velocity, the slip velocity between each elongated bubble and the surrounding liquid increases, improving the convective heat transfer coefficient at the interface, and resulting in a slight increase of the decrease velocity of this bubble.

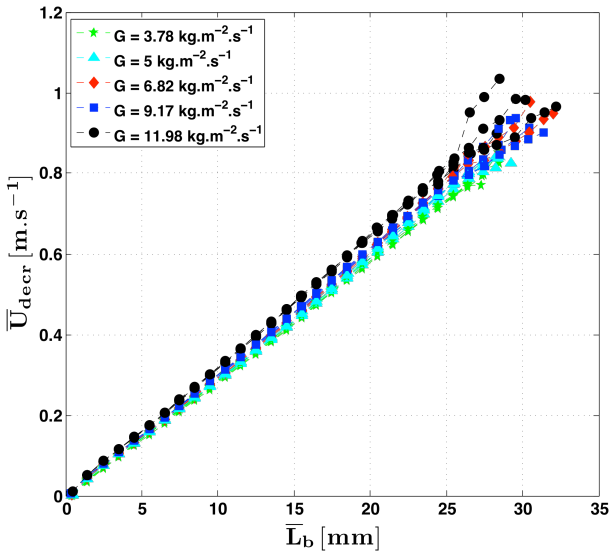

Fig. 6: Evolutions of the mean decrease velocity of the elongated bubbles as a function of their mean length for different mass velocities of the n-pentane.

As the mean decrease velocity of the elongated bubbles is proportional to their mean length, the mean latent heat flux density released by the condensation of these bubbles seems to be independent of their size. In order to demonstrate this hypothesis, the figure 7 shows the evolutions of the mean latent heat flux density released by the condensation of the elongated bubbles as a function of their mean surface for all the mass velocities of the n-pentane. For each mass velocity of the n-pentane, the mean latent heat flux density released by the elongated bubbles is almost constant and independent of their mean surface. So, the condensation kinetics of these bubbles is proportional to the heat exchange (i.e. interface) surface. Moreover, the mean latent heat flux density over the total surface of the elongated bubbles is nearly equal of the imposed heat flux density at the channel walls. Indeed, the latent heat flux density released by the bubbles is in absolute value lower by 20 % than the heat flux density imposed by the external limiting heat transfer. Considering the uncertainty of the external heat transfer coefficient (of 15 %) and the heat powers evacuated laterally through the spherical menisci closing the elongated bubbles, we can demonstrate that the external limiting heat transfer governs the condensation kinetics of these bubbles.

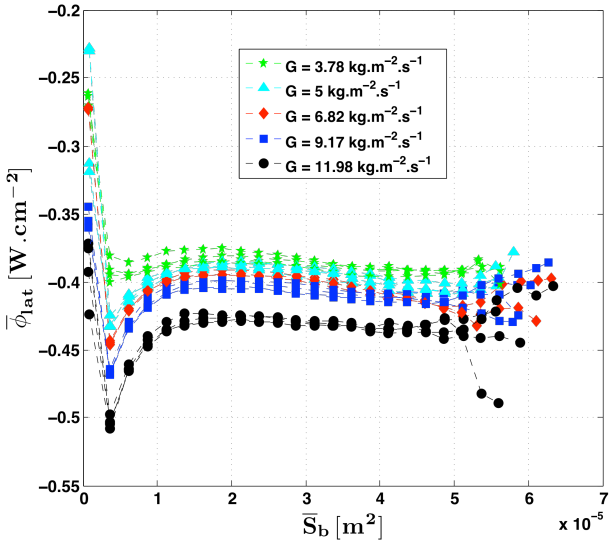

Fig. 7: Evolutions of the mean latent heat flux density released by the condensation of the elongated bubbles as a function of their mean surface for different mass velocities of the n-pentane.

For the same reasons mentioned previously, the mean latent heat flux density released by the elongated bubbles increases slightly in absolute value with the increase of the n-pentane mass velocity. It should be noted that, for mean bubbles surfaces lower than 10 mm^2,

the mean latent heat flux density presents a peak. This aspect corresponds to the transition between the intermittent zone and the spherical bubbles zone. Beyond this transition, where the spherical bubbles number becomes greater than the elongated bubbles number, the mean latent heat flux density decreases sharply in absolute value and approaches to zero in the spherical bubbles zone.

Conclusions

The condensation flows of the n-pentane at low mass velocities in an air-cooled square cross-section micro-channel, having an inner edge of 553 mm, can be divided into three main zones: the annular zone, the intermittent zone and the spherical bubbles zone. A specific experimental procedure based on the Lagrangian bubbles tracking was developed in order to determine the hydraulic and thermal parameters in the intermittent zone. Proportional relationships were found between the mean displacement and condensation velocities of the elongated bubbles and their mean length. An enhancement role of the n-pentane mass velocity increase on the elongated bubbles mean displacement and condensation velocities was highlighted. Besides, an independence between the mean latent heat flux density released by the condensation of the elongated bubbles and their mean surface was found, with an enhancement role of the n-pentane mass velocity increase. Finally, the mean latent heat flux density released by the condensation of the elongated bubbles was compared to the imposed heat flux density, showing that the condensation kinetics of these bubbles is governed by the external limiting heat transfer.

Acknowledgements

Financial supports from the FNRAE (MATRAS) and from the ESA (ENCOM) are gratefully acknowledged.

Nomenclature

G	mass velocity	$kg.m^{-2}.s^{-1}$
L	length	m
$\overline{L}$	mean length	m
$\overline{S}$	mean surface	m^2
t	time	s
$\overline{U}$	mean velocity	$m.s^{-1}$
y	vertical position in the micro-channel	pixel
z	axial position in the micro-channel	pixel

Greek symbols

$\overline{\phi}$	mean heat flux density	$W.m^{-2}$

Subscripts

b	bubble
$decr$	decrease
lat	latent

References

[1] Coleman, J.W. and Garimella, S., 2003. Two-phase flow regimes in round, square and rectangular tubes during condensation of refrigerant R134a, Int. J. Refrigeration 26, 117-128.

[2] El Achkar, G., Lavieille, P., Lluc, J. and Miscevic, M., 2011. Heat transfer and flow distribution in a multichannel microcondenser working at low mass fluxes, Int. J. Heat Mass Transfer 54, 2319-2325.

[3] El Achkar, G., Lavieille, P. and Miscevic, M., 2012. Loop heat pipe and capillary pumped loop design: about heat transfer in the isolated bubbles zone of condensers 33-34, 253-257.

[4] El Achkar, G., Miscevic, M., Lavieille, P., Lluc, J. and Hugon, J., 2013. Flow patterns and heat transfer in a square cross-section micro condenser working at low mass flux 59, 704-716.

[5] El Hajal, J., Thome, J.R. and Cavallini, A., 2003. Condensation in horizontal tubes, part 1: two-phase flow pattern map, Int. J. Heat Mass Transfer 46, 3349-3363.

[6] Garimella, S., Killon, J.D. and Coleman, J.W., 2003. An experimental validated model for two-phase pressure drop in the intermittent

flow regime for noncircular microchannels, J. of Fluids Engineering 125, 887-894.

[7] Hu, J.S. and Chao, C.Y.H., 2007. An experimental study of the fluid flow and heat transfer characteristics in micro-condensers with slug-bubbly flow, Int. J. Refrigeration 26, 117-128.

[8] Louahlia-Gualous, H. and Mecheri, B., 2007. Unsteady steam condensation flow patterns inside a miniature tube, Applied Thermal Engineering 27, 1225-1235.

[9] Médéric, B., Miscevic, M., Platel, V., Lavieille, P. and Joly, J-L., 2004. Experimental study of flow characteristics during condensation in narrow channels: the influence of the diameter channel on structure patterns, Superlattices and Microstructures 35, 573-586.

[10] Médéric, B., Lavieille, P. and Miscevic, M., 2006. Heat transfer analysis according to condensation flow structures in a minichannel, Experimental Thermal Fluid Science 30, 785-793.

[11] Odaymet, A. and Louahlia-Gualous, H., 2012. Experimental study of slug flow for condensation in a single square microchannel, Experimental Thermal Fluid Science 38, 1-13.

[12] Wu, H.Y. and Cheng, P., 2005. Condensation flow patterns in silicon microchannels, Int. J. Heat Mass Transfer 48 (11), 2186-2197.